

Using representative synthetic data to analyze effects of filters when processing full waveform airborne TEM data

Combrinck, M.^[1]

1. New Resolution Geophysics, South Africa

OUTLINE

Airborne time domain electromagnetic (ATEM) surveys have reached the stage where full waveform streamed data are recorded and delivered in addition to traditional survey products. One result of this advance in technology is that the line between the acquisition and processing phases has become more flexible and many parameters that used to be hardwired in acquisition can now be adapted during the processing phase. In order to make use of this opportunity the interpreter needs a clear description and understanding of the system specific corrections required to isolate geological responses as well as the effects of filters and other digital signal enhancement options that are available.

Validating procedures on a synthetic data set is one way of ensuring that all geological responses falling within similar parameter ranges would be accurately presented after processing. In this study the effects of three time-series and four spatial filters were analyzed. Streamed full waveform data were simulated by adding measured high altitude data to synthetic models. The various filters were applied and the deviations from the true models compared with that of the unfiltered data. The results were evaluated based on whether the filtered results showed more or less deviation than the unfiltered data from the original noise-free models.

INTRODUCTION

Converting streamed TDEM data into profiles requires a number of processing steps. These steps vary from system to system depending on the waveform, geometry and contractor preferences. Processing steps can be viewed either as corrections or filters. Corrections are procedures applied to remove any parts of the measured data that are systematic, predictable and not due to the earth's conductivity response. Filters are used to enhance the signal to noise ratio of the measured secondary field based to enhance signal to noise ratios and visual appearance of data. There are overlaps of course, for example in the case where applying a correction requires the use of a filter.

Typical corrections that are applied to recorded data to provide time gate profiles are:

- Subtracting adjacent opposite cycle 50Hz/60Hz measurements to remove 50Hz/60Hz as well as DC or very low frequency signal (Macnae et al., 1984)
- Removing system response
- Normalizing for peak current variations
- Gating of streamed data

The application details of these corrections vary from system to system, based on the configuration central loop vs towed bird) and waveform (full duty cycle vs partial

duty cycle). Few end users of ATEM data would likely be in a position to know all different systems intimately enough to add this level of processing to their interpretation flows.

Filters, on the other hand, can readily be applied by interpreters to highlight their specific targets of interest and are largely independent of the system. With the advent of streamed data recording, the potential is there for interpreters to get access to data that is much less filtered than in the past, providing them with more flexibility to apply filtering routines of their own design.

Most filters are effective in improving precision and making data more visually appealing, but the question is what the cost is in terms of accuracy. This paper focuses on a variety of commonly used filters both in the time and spatial domains, and quantify what the effects are on the accuracy of the final results.

FILTER DESCRIPTIONS

The filters that were investigated in this study, are divided into time series and spatial categories and summarized as follows.

Time series filters

In cases where streamed data are not recorded these filters are applied electronically and in the analog domain during the acquisition phase. Recorded full waveform data enables us to better evaluate and design these filters.

- **Despiking**

The despiking filter was developed very specifically for streamed TDEM data processing based on the observed characteristics of spheric noise (Fig. 1). Spheric events tend to occur over 200 to 500 samples (6.4 μ s sampling interval), and although there is often a single peak that can be identified, the data are corrupted for up to 500 samples surrounding the peak. Even if 500 samples are corrupted, that is less than a quarter of the recorded decay. The despiking filter is designed to identify these spikes and only interpolate the affected part of the data stream from adjacent stations. Filter sensitivity is based on average noise levels determined from high altitude measurements.

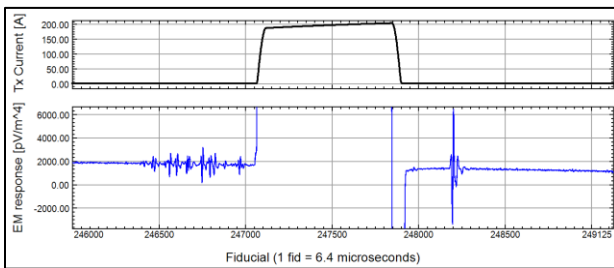


Figure 1: Example of two events of spheric noise. The top panel shows the transmitter current as reference and the bottom panel shows the recorded streamed data over 3125 fiducials or 20ms. The first spheric event is recorded just before the transmitter current is switched on and the second shortly after the turn-off.

- **Low Pass Finite Impulse Response (FIR)**

FIR filters are applied by convolving a finite number of coefficients with a time series. The number of coefficients (filter order plus one) and coefficient values are the variable parameters. A series of low pass filters between 5 kHz and 15 kHz were designed using the Parks-McCellan algorithm and applied in Oasis Montaj using a custom executable file (gx).

- **Variable Width Averaging (VWA)**

The VWA filter was inspired by the concept of variable width gates used in most, if not all, time domain EM systems. Time gates (or channels) are chosen to be small in early times where the signal to noise ratio is high and the decay changes rapidly with time. They are then progressively widened with time until many streamed data samples are averaged to produce a single channel where the signal to noise ratios are lower and the decay slope much less than at early times. The VWA filter uses the same principle and averages values along the times series using single data samples at positions where the decay rapidly changes and larger averaging widths where the decay flattens out. The main difference between this filter and the normal gating procedure is that there is no

reduction in the number of data points between input and output, whereas gating would typically reduce 2000 points to 50 or less. The VWA filter is also applied in Oasis Montaj using a custom executable file (gx).

Spatial filters

- **FFT low pass**

The FFT low pass filter was applied using Oasis Montaj software. The filter is based on the method described by Fraser et al. (1966) and the only variable parameter is the filter cut-off wavelength.

- **Stacking (averaging)**

The stacking or averaging filter calculates the average of a specified number of samples with equal weight assigned to each sample. The only variable parameter is the number of samples.

- **Non-linear**

The non-linear filter was also applied using Oasis Montaj software. This filter was first described by Naudy and Dreyer (1968) and has two variable parameters; the filter width as well as filter tolerance or noise amplitude.

- **Polynomial fitting (Savitzky-Golay)**

The Savitzky-Golay filter is based on fitting successive subsets of adjacent data points with a polynomial by the method of linear least squares (Savitzky and Golay, 1964). A stand-alone algorithm was used to implement this filter with variable parameters being the filter width and the order of polynomial to use.

METHODOLOGY

Synthetic data were calculated using 200m x 200m and 400mx400m plates with conductances scaled so that the decay constants (τ) was 1ms and 5 ms for each of the two plates. Two sections of data measured at high altitude during an Xcite™ test survey in Ermelo, South Africa were used as typical examples of AEM noise. One section, referred to as the “low noise” section was acquired during optimal survey conditions while the “high noise” section was acquired during less than ideal conditions with a thunder storm approaching (Fig. 2).

Maxwell modelling software that was used to calculate the theoretical plate responses does not allow the calculation of more than 3000 gates which is typical for streamed data systems. In order to generate typical model responses Maxwell was used to calculate the standard off-time responses for a variety of different plate sizes and depths.

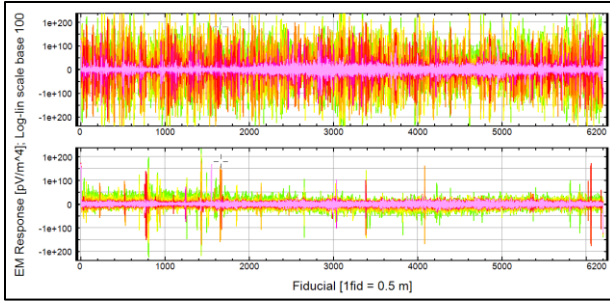


Figure 2: Profiles of “low noise” (bottom) and “high noise” (top) sections after standard processing.

The conductivities were chosen to give predetermined decay constant values of 1ms and 5ms which are typical values that can be detected with 25Hz off-time helicopter TDEM systems (reference relationship between tau and geometry). Streamed data responses for these decay constants were calculated by convolving a measured system waveform (Combrinck and Wright, 2016) over ten full waveform cycles with exponential functions of the form:

$$F_{\tau_i}(t) = e^{-t/\tau_i} ; i = 1,5 \quad (1)$$

These responses are late time approximations and not accurate for early times, but are sufficient for the purpose of investigating filter effects in the mid- to late time range (>170 ms) after turn-off. The full waveform responses for each decay constant were then scaled to match the plate modelling software at the overlapping time gates to account for plate and system geometry and create streamed data profiles of synthetic data.

Noise sections were added to the model data to give representative streamed data sets and the minimum corrections mentioned in the previous section were applied to each of these. The noise sections were also processed on their own as separate lines.

In the next phase the different filters (with a range of parameters) were applied to the modelled data with noise added, as well as to the noise sections alone.

Standard deviations over 300 points of the noise were used as estimates of precision for each instance of a filter. Similarly, standard deviations of the filtered data from the model data (before any noise were added) over 300 points were used as estimates for accuracy (Eq. 2).

$$StdDev(F(x)) = \sqrt{\frac{1}{n} \sum_{i=1}^n (x_i - \mu_i)^2} \quad (2)$$

where,

$$\begin{aligned} n &= 300, \\ \mu_i &= \text{model value without noise added} \\ x_i &= \text{filtered data} \end{aligned}$$

RESULTS

The synthetic data combinations were split into 10 lines labelled as follows:

HN: High noise section, no plate

HN_200_1: 200x200m plate; $\tau = 1$ ms; high noise added

HN_200_5: 200x200m plate; $\tau = 5$ ms; high noise added

HN_400_1: 400x400m plate; $\tau = 1$ ms; high noise added

HN_400_5: 400x400m plate; $\tau = 5$ ms; high noise added

LN: Low noise section, no plate

LN_200_1: 200x200m plate; $\tau = 1$ ms; low noise added

LN_200_5: 200x200m plate; $\tau = 5$ ms; low noise added

LN_400_1: 400x400m plate; $\tau = 1$ ms; low noise added

LN_400_5: 400x400m plate; $\tau = 5$ ms; low noise added

Each of these lines have been processed with the minimum corrections required to extract 32 gated profiles. The profile data for these 10 lines are shown in Figure 3. Subsequent comparisons always used these 10 lines as reference. Standard deviations were calculated over all stations on all lines, but two locations highlighted on each line were used to draw comparisons between the various filters.

Combining all the filter variations resulted in 57 sets of filtered data. Only a few selected examples will be discussed to illustrate the effects of each filter and the standard deviations of each results from the original models will be used as a more comprehensive comparison tool to include all the data.

Time series filters

- Despiking

A profile example of the despiking filter applied to the low noise case is shown in figure 4. The larger amplitude spikes have been successfully removed and the effect of this filter is limited to the spherical affected decays only, unlike a typical frequency domain filter which affects all the data. In figure 5 we have the same filter applied to a high noise line. The only difference is that the filter sensitivity was adjusted to match the higher standard deviation of the noise. The despiked profiles are smoother, especially over the plate anomaly. The general nature of the profiles is still very noisy and on closer inspection a few samples can be found where spikes were introduced and worsened the data. This

filter performed better in the low noise case as it is based on finding single station sharp variations (spherics) in a more homogeneous background. The high noise case does not conform to this basic assumption as the spheric activity dominates the data. As mentioned, this noise sample was collected as a thunder storm was approaching and even though the despiking filter is designed to deal with spheric activity it will underperform if the spheric interference is continuous or have events that are too close in time to be treated as individual spikes.

The profile presentation used in figures 4 and 5 are useful to indicate smoothness of data and provide a qualitative sense of noise reduction. The next step is to quantify the filter results in terms of the standard deviation of the filtered data from the noise-free model data. The standard deviation is calculated for each channel over 300 points or 150m. This standard deviation (error) for each filtered channel is then expressed as a fraction of the error of the unfiltered data. In this format values smaller than one indicate that the filter has improved the data and values larger than one indicate that the error has increased. So, even though profiles might appear smoother, the filtered data could be less accurate when compared with the original models. Figure 6 shows the error fractions of the two lines from figures 4 and 5, calculated at the stations indicated with the black dots. The profiles marked with “b” at the end always correspond to the second station on the line counting from the left. Although these stations are indicated as single dots, the errors are calculated for the 300 points surrounding each one, and the profiles are therefore representative of more than a single decay.

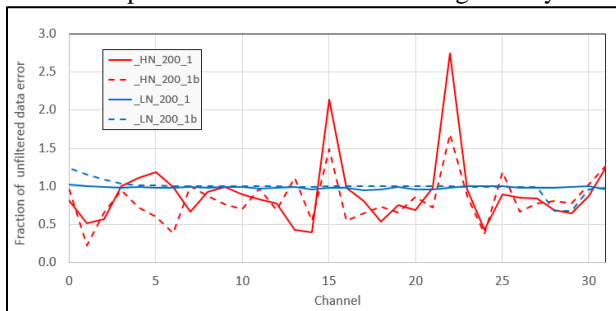


Figure 6: The error fractions for lines HN_200_1 and LN_200_1 at two stations on each line.

The low noise line show very little variation from one except on the first and last three channels of LN_200_1_b. The reduction in error of the last three channels corresponds to a late time spike that was successfully filtered out. The spike is visible on Figure 4 just to the right of the second marked station (black dot). The increase in error in the early channels is not immediately evident and the reason is addressed in a subsequent paragraph.

The high noise line show improvements on most channels, but not all. Channels 15 and 23 were made worse in both example stations. The presentation in figure 6 is useful, but limited with the number of models that can be compared. In order to illustrate the effect of the despiking filter on all the models (2 stations on 10 lines) the average of the error fraction over the 32 channels are calculated and displayed as a function of the line and center station (Figure 7).

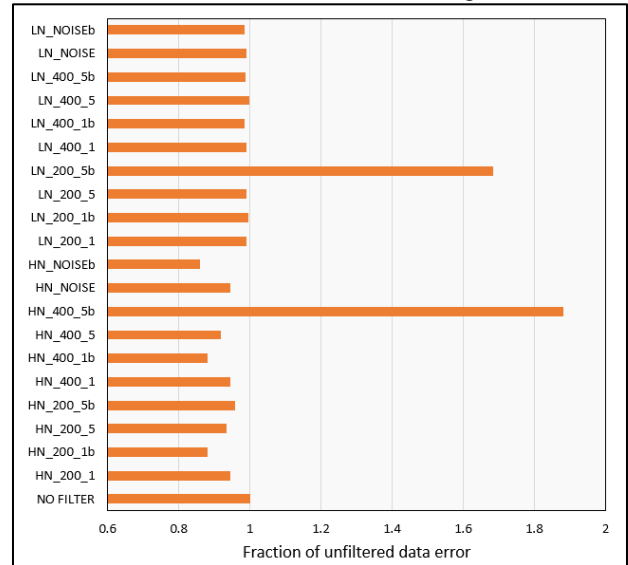


Figure 7: The average error fractions of the despiking filter for all model lines and stations.

Apart from LN_200_5b and HN 400_5b it is clear that the low noise lines are generally slightly improved, and that the high noise lines are improved on average, even if not for every channel individually. Closer inspection of LN_200_5b and HN 400_5b revealed that the anomaly peak curvatures were so sharp that they were treated as spikes as well. This also happened on some of the other lines and was the reason for the first three channels in Figure 6 to have error fractions more than one. However, on LN_200_5b and HN 400_5b the majority of channels were picked as spikes resulting in an average error fraction larger than one.

- FIR

Fifteen instances of the FIR filter were tested in total Filters were designed to have cut-off frequencies of 5, 10 and 15 kHz. In a first run, each of these frequencies were implemented with 6, 11 and 16 coefficients corresponding to 5th, 10th and 15th order filters. The results from this first attempt indicated that the filters using an even number of points (5th and 15th order) introduced much larger errors than the 10th order filter for the same cut-off frequencies. One of the more extreme examples is shown in Figure 8a. The effect was more pronounced on the low noise data lines over the anomalies where the signal was strongest. It

reflects the error introduced by the asymmetry of even point filters, especially where steep slopes on decays are encountered.

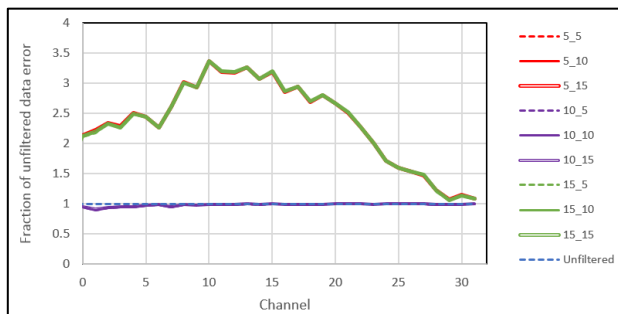


Figure 8a: Fraction errors of 5th, 10th and 15th order FIR filters compared to unfiltered data at station LN_400_5b. In the legend the first number refers to the filter order and the second to the cut-off frequency in kHz.

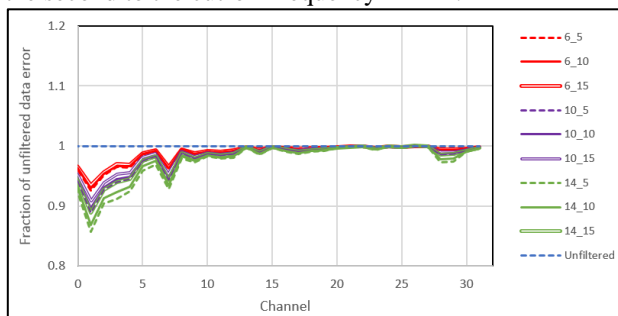


Figure 8b: Fraction errors of 6th, 10th and 14th order FIR filters compared to unfiltered data at station LN_400_5b.

A second run of filters were then applied using only uneven numbers for filter coefficients (Figure 8b). The filter order seems to have a larger effect than the cut-off frequency on reducing the error.

The results for the 5 kHz low pass instance of the 6th, 10th and 14th order filters are shown in Fig. 9. The 14th order filter has the biggest effect in reducing the error and is more effective on the high noise data. Except for the LN_200_1b line, there is always an improvement. In Fig. 10 a profile comparison of line HN_400_1 is shown with selected channels before and after the filter is applied. Compared to the despiking filter there is far less improvement in the profile smoothness, especially of the later channels. This is likely due to the fact that the later channels are already averaged extensively through the gating process and the relative small width FIR filter does not cause a significant improvement on these late channels.

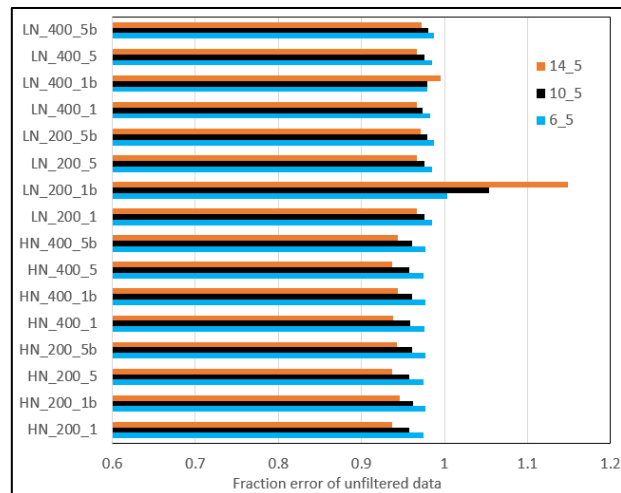


Figure 9: The average error fractions of 5kHz instance of the 6th, 10th and 14th order FIR filters for all model lines and stations.

- Varying width averaging (VWA) filter

The results from the VWA filter are presented in Fig. 11 together with the despiking filter results from Fig. 7 for comparison and a profile example of HN_400_1 is shown in Fig. 12. Comparing the profiles to the same data shown for the FIR filter in Fig.10, it is clear that the late time noise reduction is much better, while the early channel changes are a bit less. Overall though, the VWA filter gives the largest error reduction over all channels and models of the three filters discussed so far.

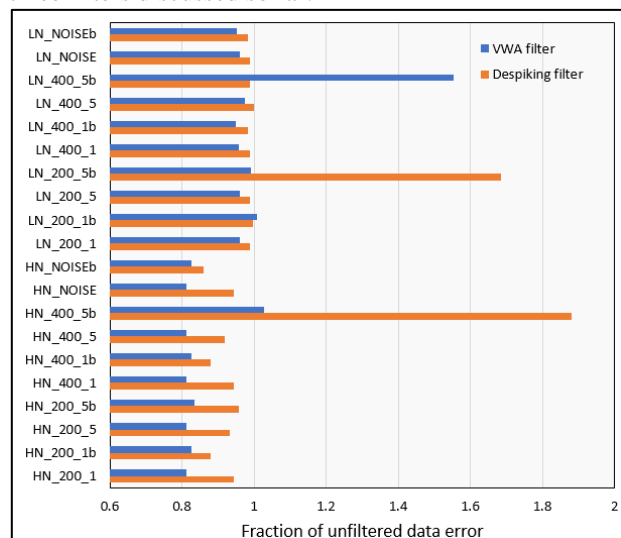


Figure 11: Average error fractions of the VWA and despiking filters for all model lines and stations.

Spatial filters

The four spatial filters all have a filter width variable. The widths for each one were changed from 21 to 201 fiducials in intervals of twenty. Although the exact effects of the filter widths are different for the different filters, it is used as a practical means to draw comparisons between the four. Figures 13-16 summarize the effects of the spatial filters on the different data sets.

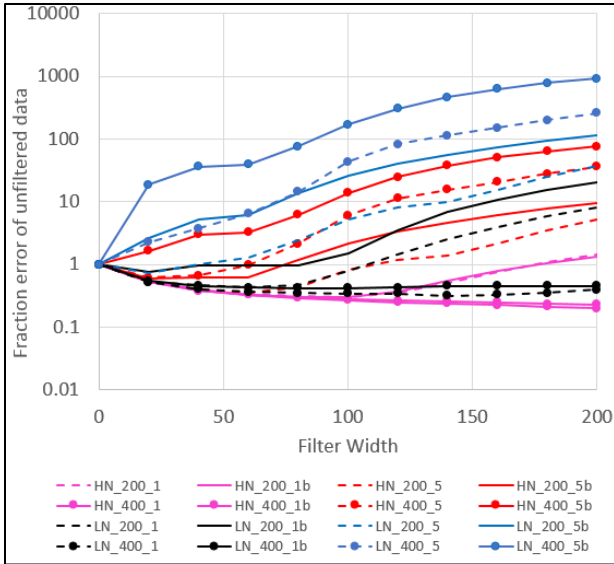


Figure 13: Average error fractions as a function of low pass filter width.

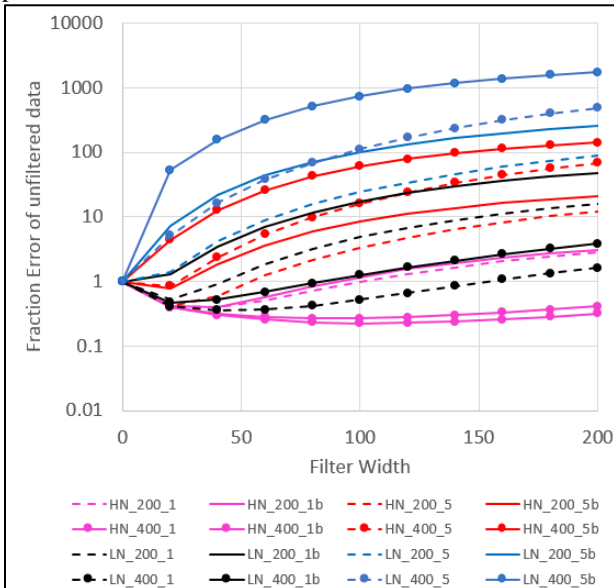


Figure 14: Average error fractions as a function of stacking filter width.

The $\tau=5$ ms conductors show the largest errors on all filters while the high noise lines with $\tau=1$ ms conductors benefit the most from filtering.

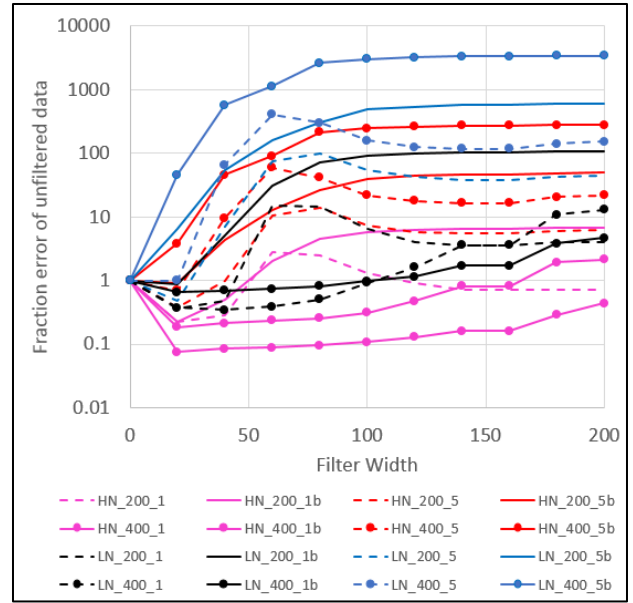


Figure 15: Average error fractions as a function of non-linear filter width.

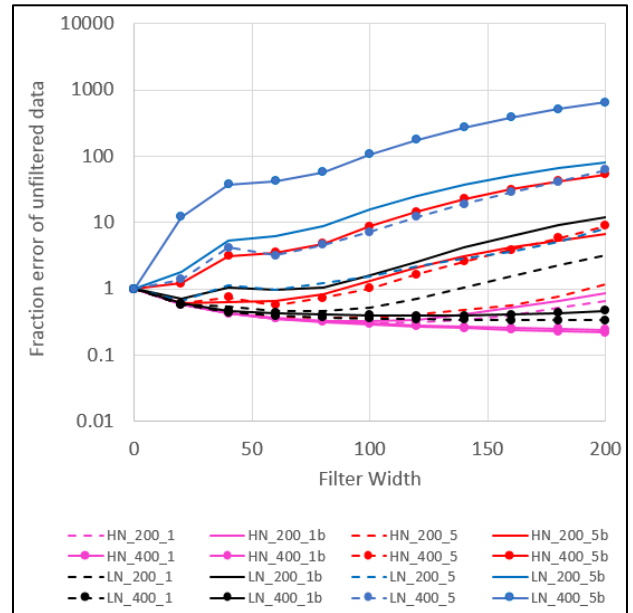


Figure 16: Average error fractions as a function of Savitzky-Golay filter width.

In most cases an initial reduction in error is observed for short filter widths and then followed by a steady increase in error with increasing filter width. The filter width where this change occurs and also the rate at which the errors increase is dependent on the filter type. In figures 17 and 18 some results are regrouped to better visualize the effects of the different filters.

In figure 17 all the low noise (LN) lines are grouped together. All these models show an increase in error with

filtering but the Savitzky-Golay filter causes the smallest error increase, closely followed by the low pass filter.

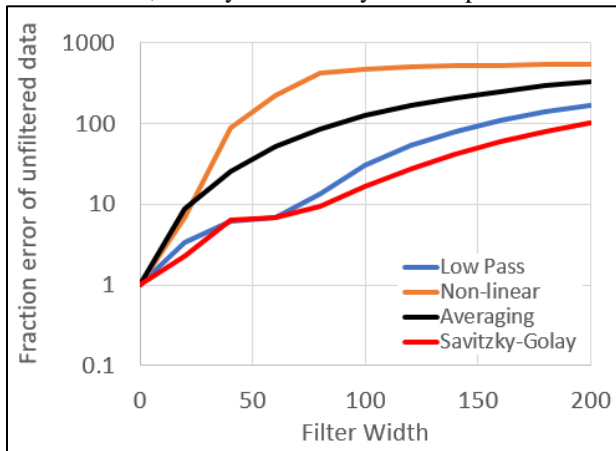


Figure 17: Average error fractions for the low noise models.

In figure 18 the high noise (HN) results are shown. With this group we see an initial error reduction for all filters. The low pass and Savitzky-Golay filters can be applied with filter widths up to 80 and 60 fids respectively before the errors start increasing.

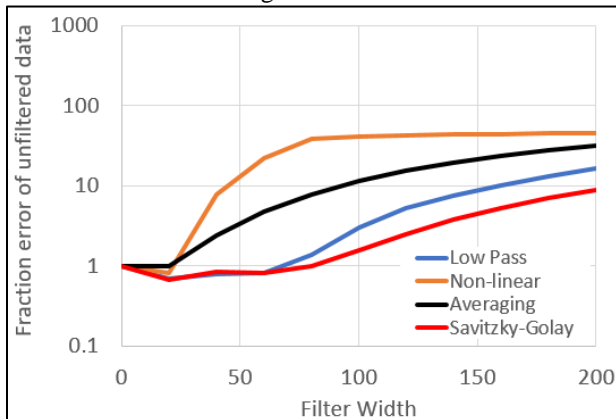


Figure 18: Average error fractions for the high noise models.

Profile comparisons of these filters are shown in figures 19 and 20 for filter widths of 101 fids. The two lines that are shown are the ones that benefited the most (HN_400_1) and the least (LN_400_5) from the spatial filters. It is interesting to note that while the non-linear filter gave the best results on HN_400_1 it also gave the worst results by far on LN_400_5.

CONCLUSIONS

Recording of streamed data in modern ATEM systems allow corrections and filters that were traditionally applied during acquisition to now be implemented in the

processing phase. As advanced filtering now becomes an optional post-acquisition procedure it is crucial for processors and interpreters to understand the effects of these filters on data.

A simple yet effective method was used to calculate errors and evaluate the effects of various filters on streamed data sets. Even though the number of filters and models included in this study are by no means representative of all options and environments it is clear that significant errors can be introduced if the only aim (and measure of success) is to provide smooth and visually appealing data. Most filters will change the input data in some way. Comparing the results from the spatial filters on high and low noise data (Figures 17 and 18) illustrates that high noise data can benefit from filtering but that low noise data do not. Of the filters examined here the VWA and the Savitsky-Golay filters showed the most promising results applied to the time series and spatial data respectively. The VWA filter is effective because it filters the high noise (late time) data more than the low noise data (early time). Developing filters that apply a similar principle in the space domain, based on data amplitudes and lateral spatial gradients could be investigated in future.

ACKNOWLEDGEMENTS

Thank you to NRG for use of streamed data samples and Richard Wright (NRG Engineering Manager) for his invaluable contributions in designing filters and developing software for this study.

REFERENCES

- Combrinck, M., Wright, R., 2016, "Achieving accurate interpretation results from full-waveform streamed data AEM surveys": ASEG_PESA 2016, Adelaide, Australia, Expanded Abstracts
- Fraser, D.C., Fuller, B.D. and Ward, S.H., 1966. "Some numerical techniques for application in mining exploration.": *Geophysics*, 31(6), 1066-1077.
- Macnae, J.C., Lamontagne, Y., and West, G.F., 1984, "Noise processing techniques for time-domain EM systems": *Geophysics* 49, 934-948.
- Naudy, H., and Dreyer, H., 1968, "Essai de filtrage non-linéaire appliqué aux profils aeromagnetiques (Attempt to apply nonlinear filtering to aeromagnetic profiles)": *Geophysical Prospecting*, 16, 171-178.
- T. W. Parks and J. H. McClellan., 1972, "Chebyshev approximation for nonrecursive digital filters with linear phase.": *IEEE Trans. on Circuit Theory*, 19:189-94.
- Savitzky, A., Golay, M.J.E. (1964). "Smoothing and Differentiation of Data by Simplified Least Squares Procedures": *Analytical Chemistry*, 36 (8): 1627-39.

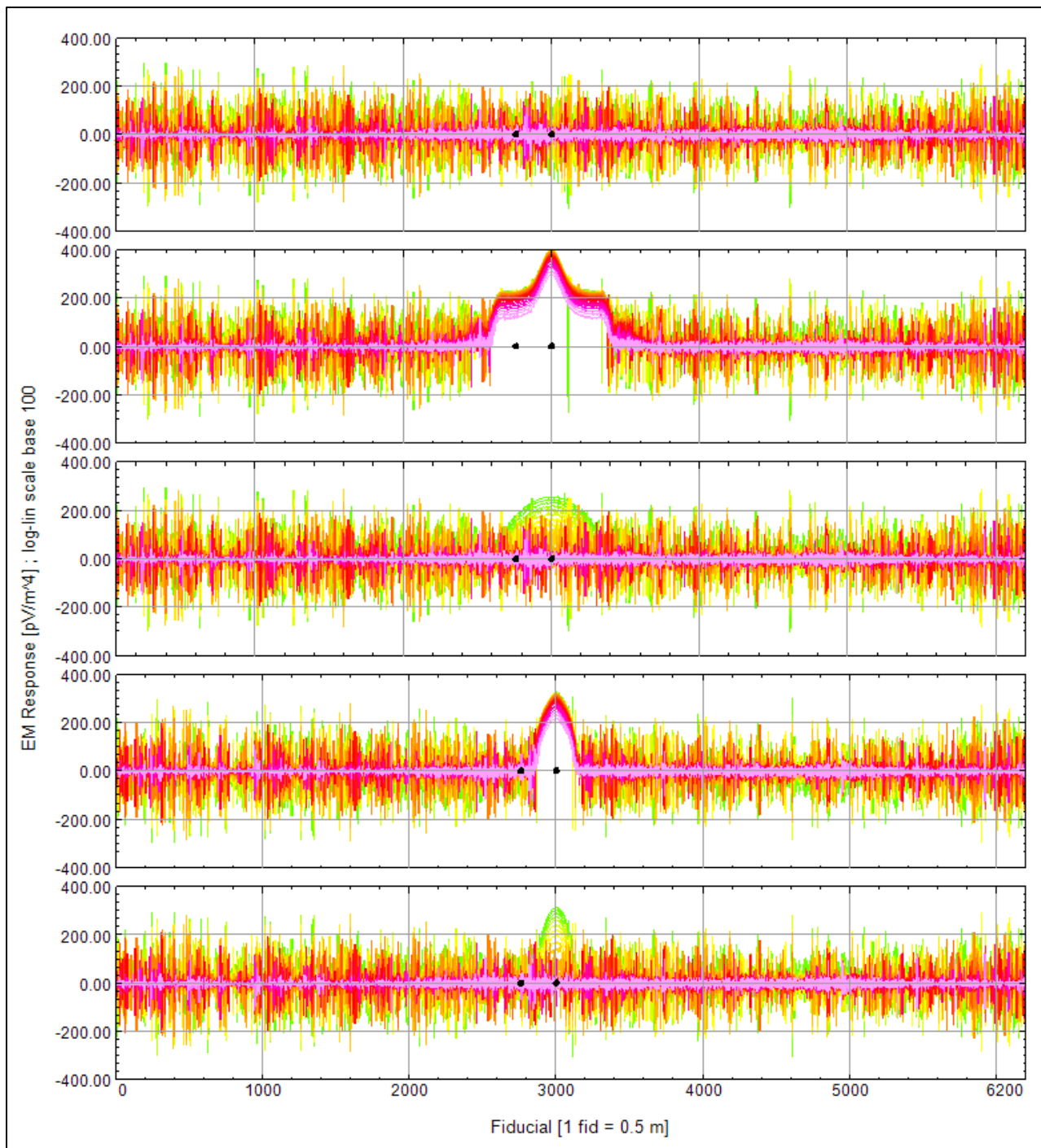


Figure 3a: Profiles of high noise lines. Panel 1: HN - High noise section, no plate. Panel 2: HN_400_5 - 400x400m plate; $\tau = 5\text{ms}$; high noise added. Panel 3: HN_400_1 - 400x400m plate; $\tau = 1\text{ms}$; high noise added. Panel 4: HN_200_5 - 200x200m plate; $\tau = 5\text{ms}$; high noise added. Panel 5: HN_200_1 - 200x200m plate; $\tau = 1\text{ms}$; high noise added. The black dots indicate the stations referenced for decay analysis and standard deviation comparisons.

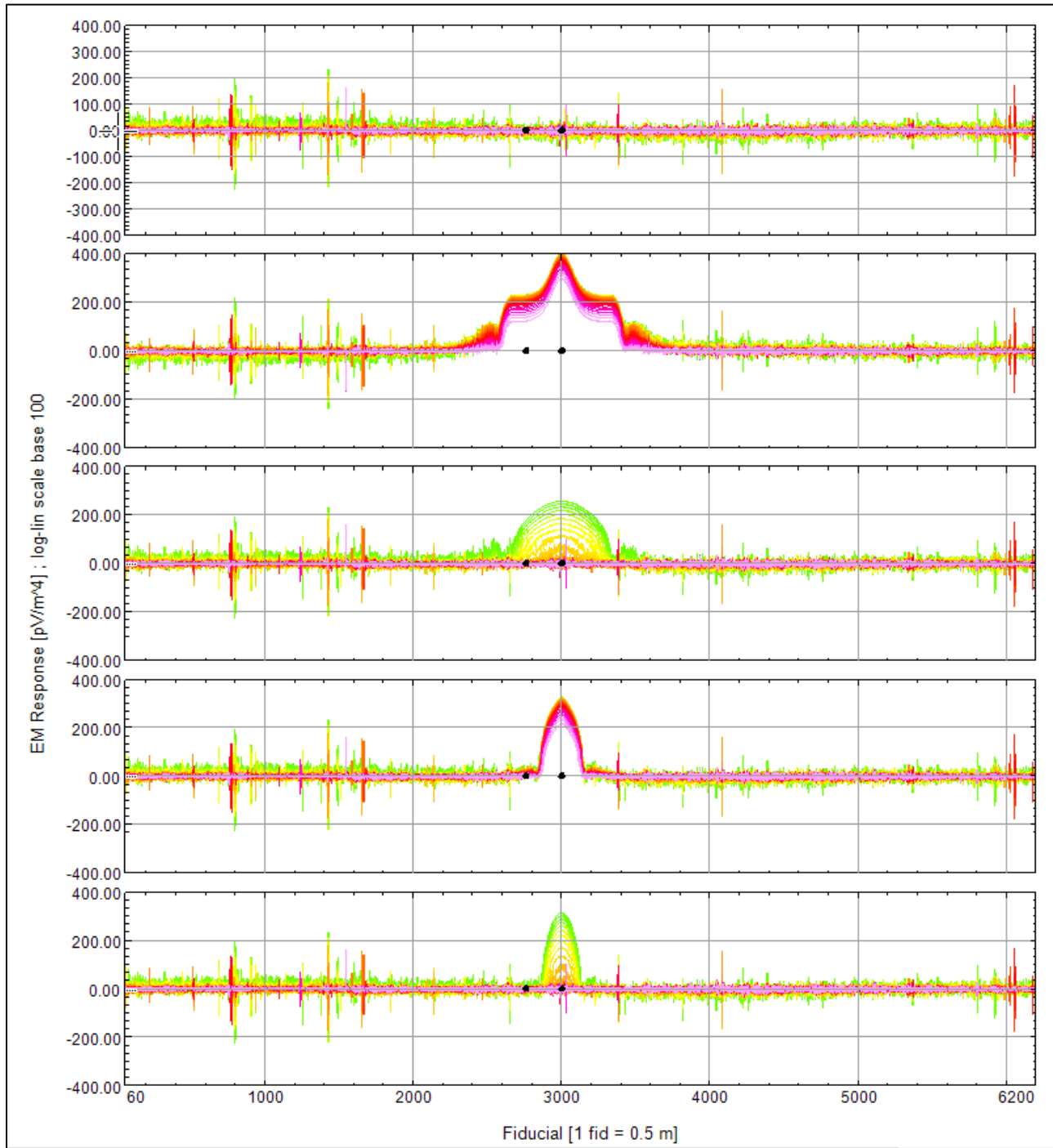


Figure 3b: Profiles of low noise lines. Panel 1: LN - Low noise section, no plate. Panel 2: LN_400_5 - 400x400m plate; $\tau = 5\text{ms}$; low noise added. Panel 3: LN_400_1 - 400x400m plate; $\tau = 1\text{ms}$; low noise added. Panel 4: LN_200_5 - 200x200m plate; $\tau = 5\text{ms}$; low noise added. Panel 5: LN_200_1 - 200x200m plate; $\tau = 1\text{ms}$; low noise added. The black dots indicate the stations referenced for decay analysis and standard deviation comparisons.

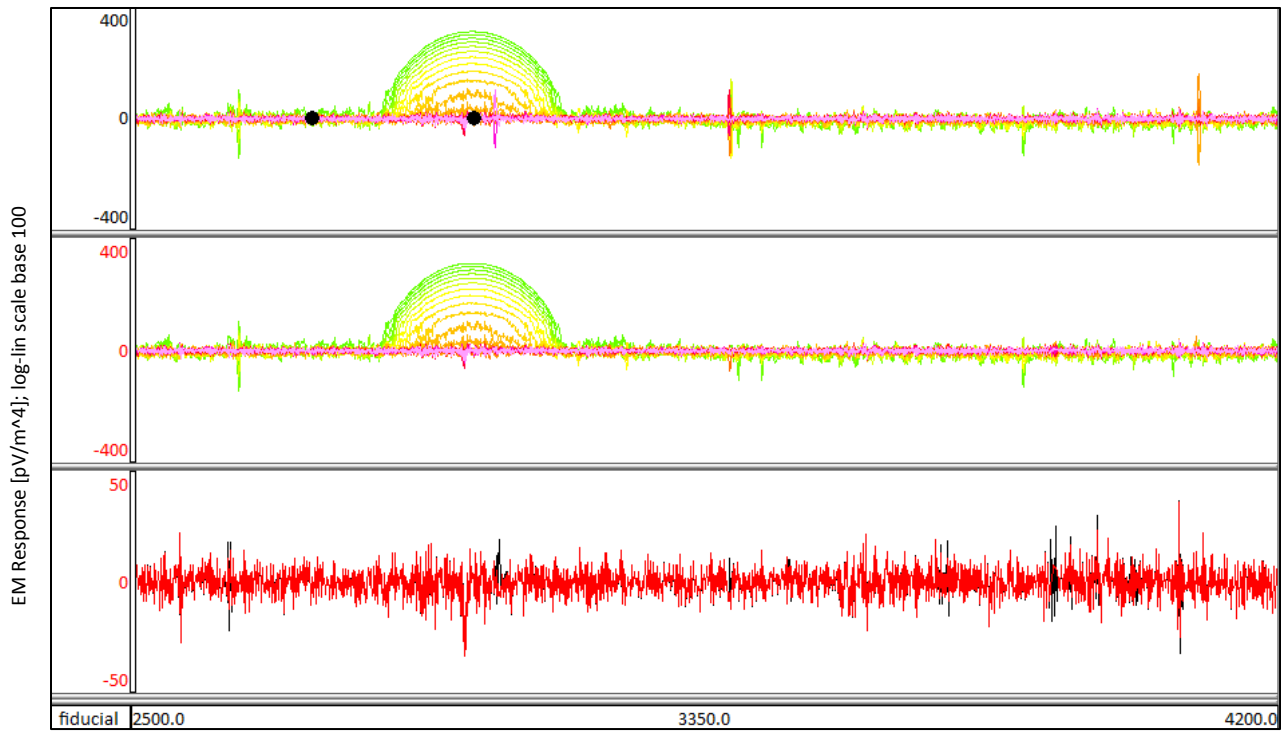


Figure 4: Low noise example of the despiking filter. A section of the line (LN_200_1) with the 200x200m plate ($\tau = 1$ ms) and low noise added is shown in the top panel. The middle panel illustrates the same channels after the despiking filter has been applied. The bottom panel compares the last channel only of the unfiltered data (black) and the despiked data (red).

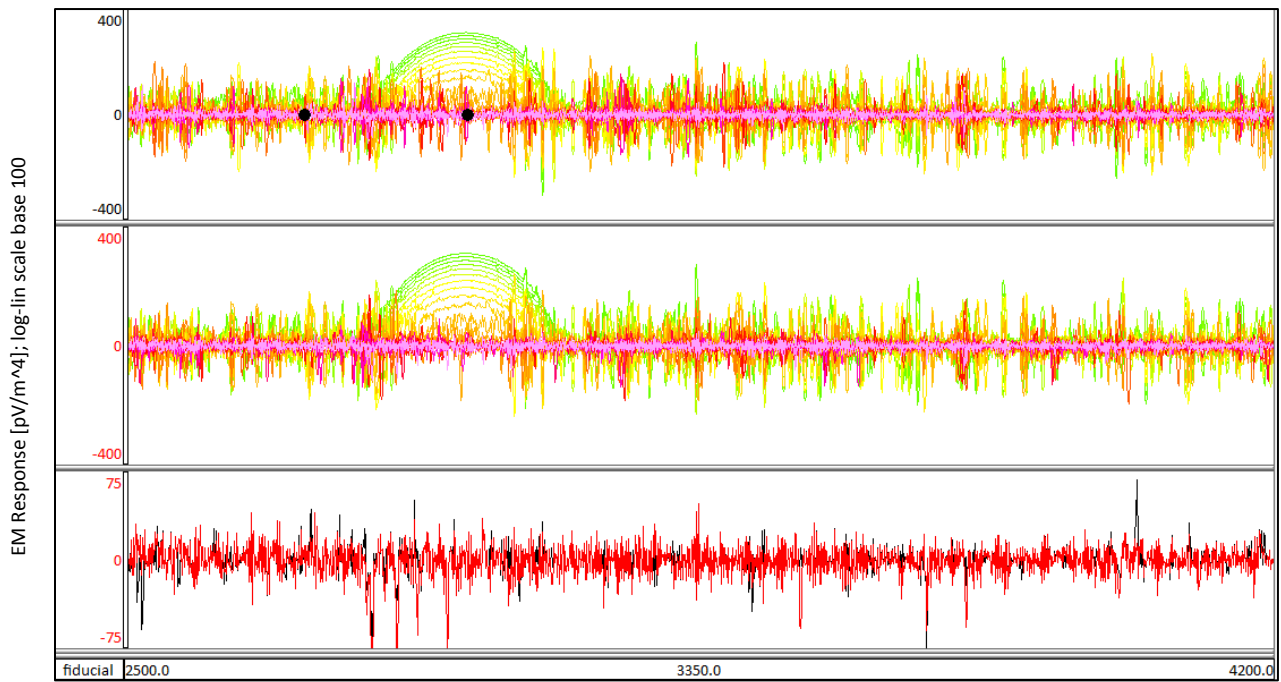


Figure 5: High noise example of the despiking filter. A section of the line (HN_200_1) with the 200x200m plate ($\tau = 1$ ms) and high noise added is shown in the top panel. The middle panel illustrates the same channels after the despiking filter has been applied. The bottom panel compares the last channel only of the unfiltered data (black) and the despiked data (red).

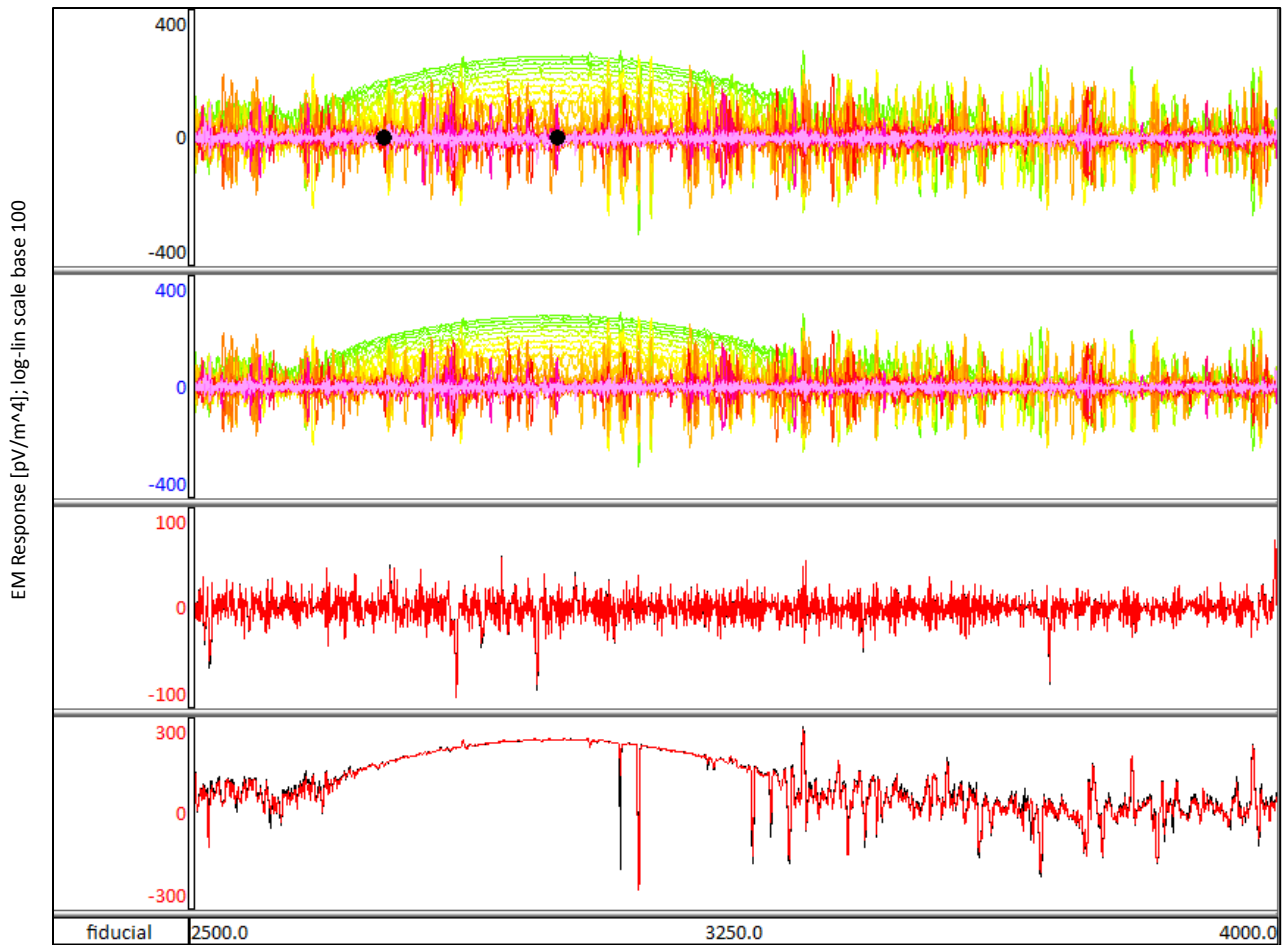


Figure 10: High noise example of the 5kHz low pass, 14th order FIR filter. A section of the line (HN_400_1) with the 400x400m plate ($\tau = 1$ ms) and high noise added is shown in the top panel. The second panel illustrates the same channels after the FIR filter has been applied. The third panel compares the last channel only of the unfiltered data (black) and the filtered data (red). The bottom panel shows the third channel of the unfiltered data (black) and the filtered data (red).

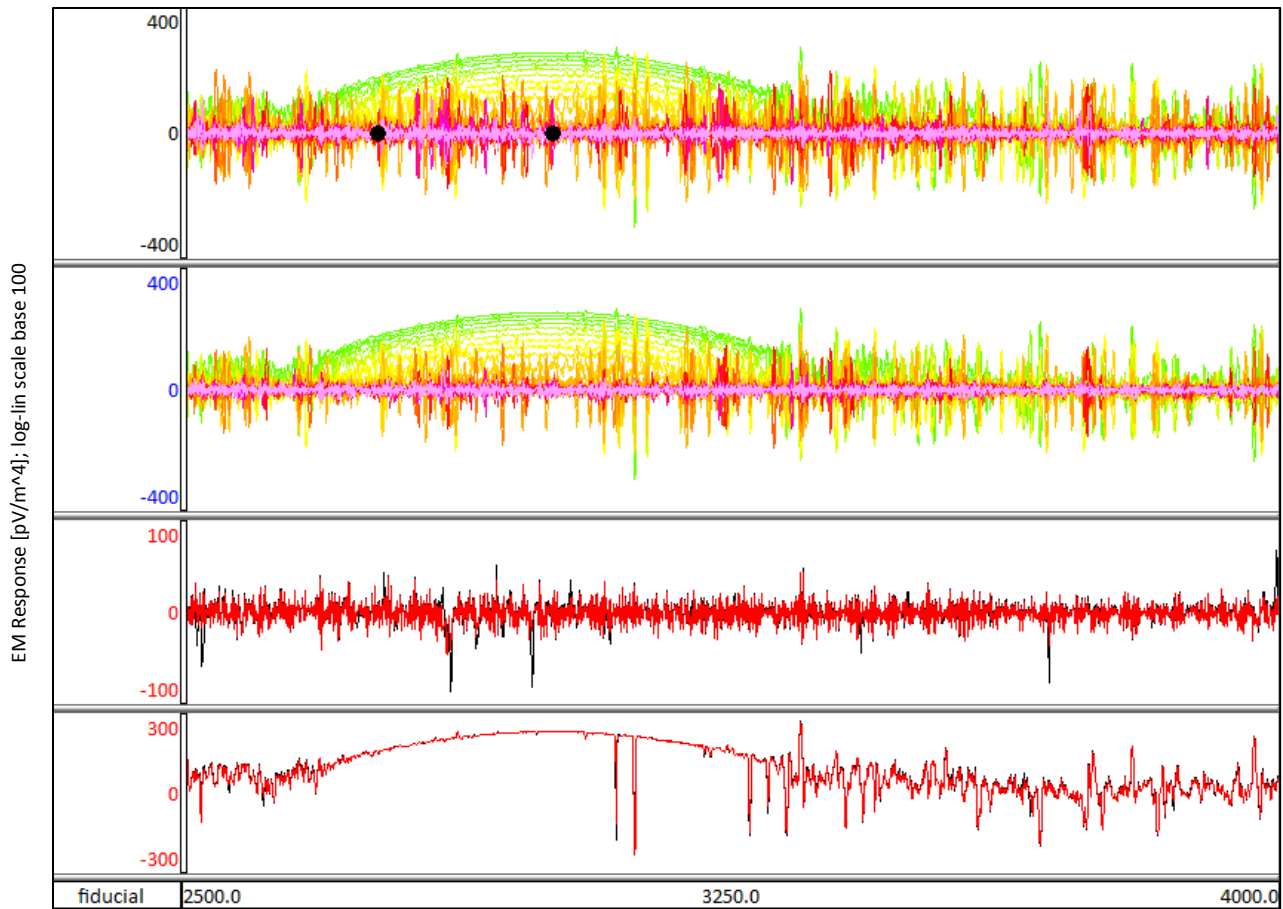


Figure 12: High noise example of the VWA filter. A section of the line (HN_400_1) with the 400x400m plate ($\tau = 1$ ms) and high noise added is shown in the top panel. The second panel illustrates the same channels after the VWA filter has been applied. The third panel compares the last channel only of the unfiltered data (black) and the filtered data (red). The bottom panel shows the third channel of the unfiltered data (black) and the filtered data (red).

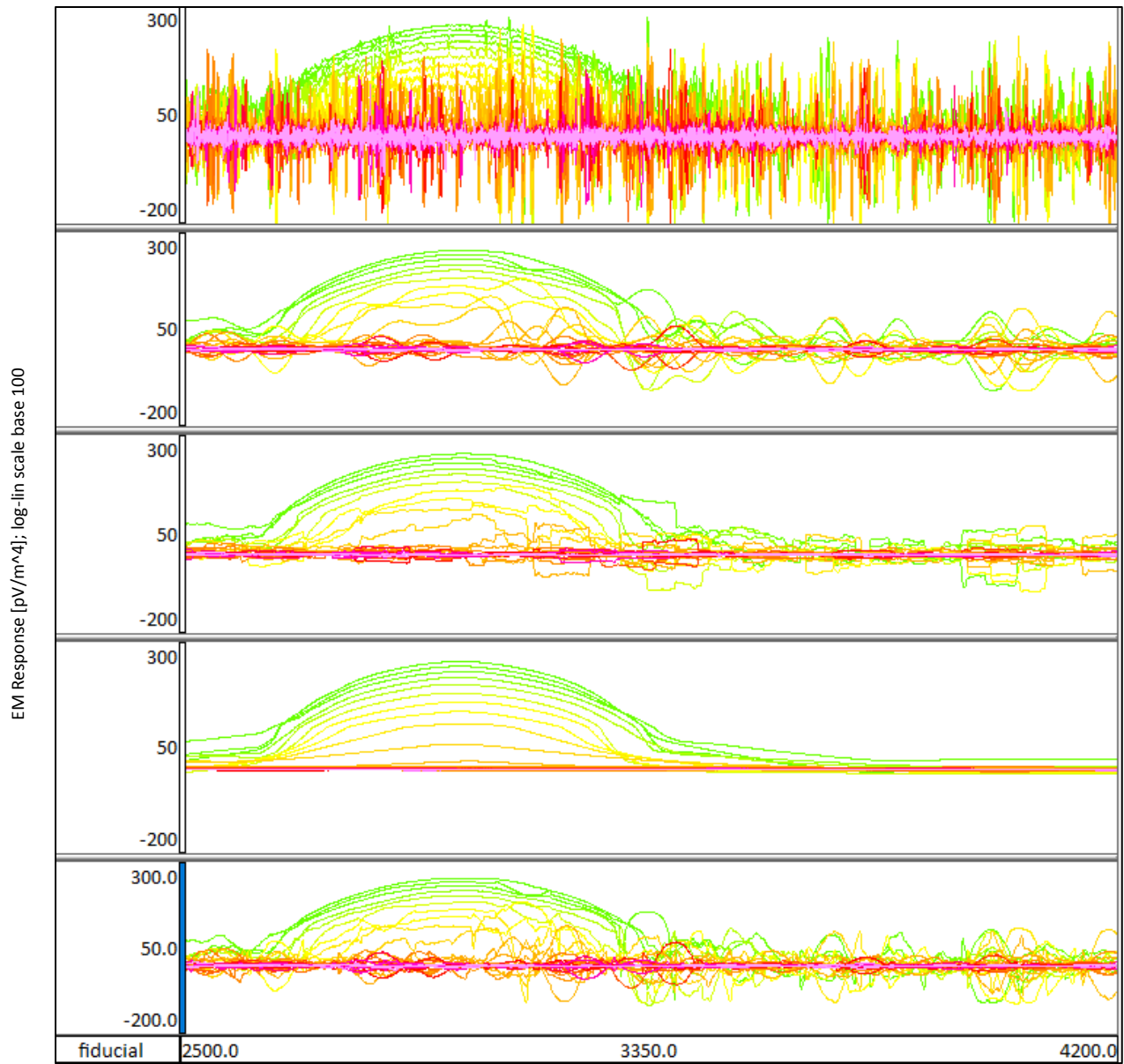


Figure 19: The effects of the four spatial filters with filter width 101 fiducials (= 50m) on line HN_400_1 are shown. Top Panel: Unfiltered data. Second Panel: Low pass filter. Third Panel: Stacking (averaging) filter. Fourth Panel: Non-linear filter. Fifth Panel: Savitsky-Golay filter.

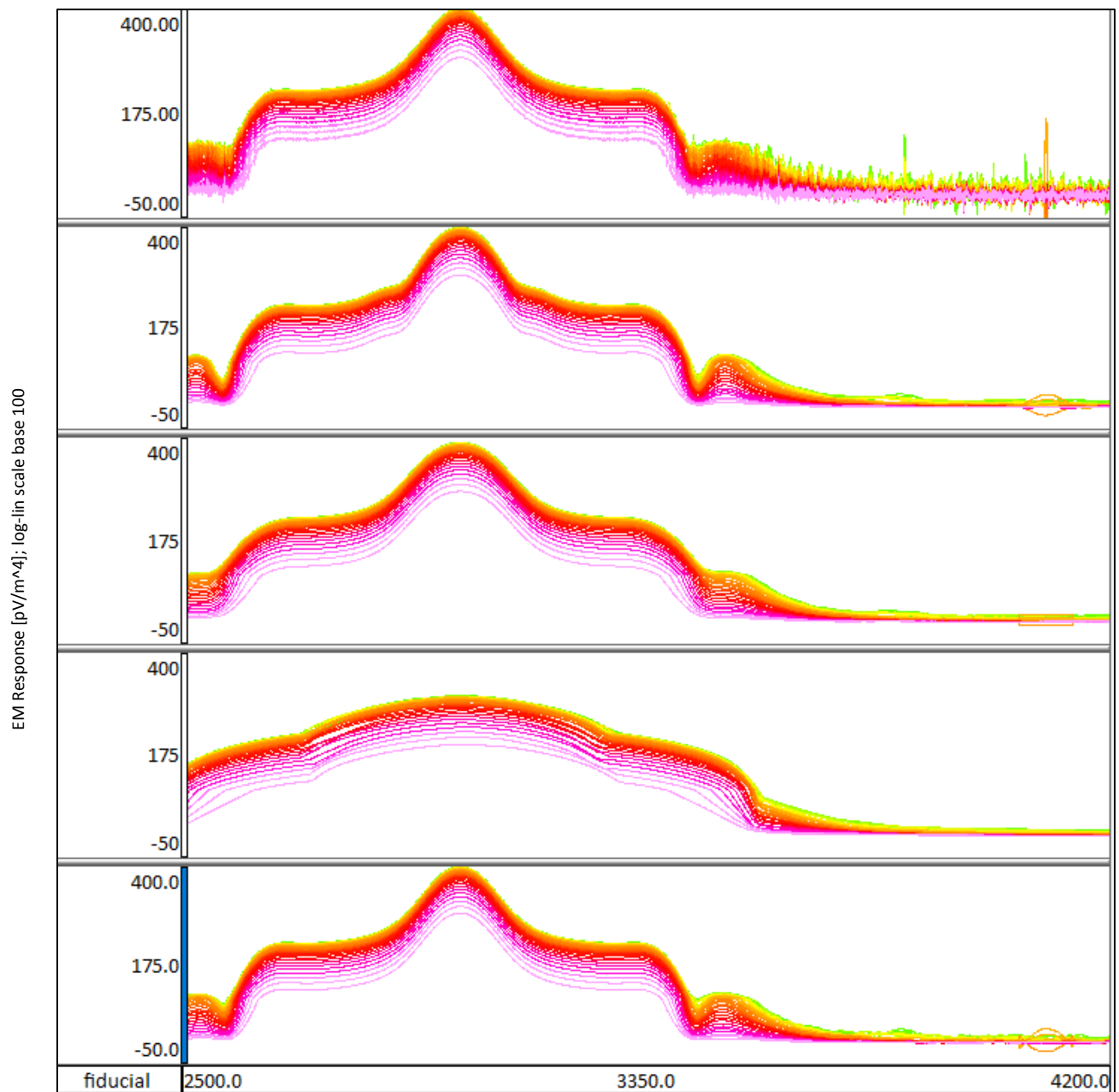


Figure 20: The effects of the four spatial filters with filter width 101 fiducials (= 50m) on line LN_400_5 are shown. Top Panel: Unfiltered data. Second Panel: Low pass filter. Third Panel: Stacking (averaging) filter. Fourth Panel: Non-linear filter. Fifth Panel: Savitsky-Golay filter.